A one-dimensional model of a false aneurysm

Berntsson Fredrik, Matts Karlsson, Vladimir Kozlov and Sergey A. Nazarov

Fredrik, B., Karlsson, M., Kozlov, V., Nazarov, S. A., (2017), A one-dimensional model of a false aneurysm, *International Journal of Research in Engineering and Science (IJRES)*, 5(6), 61-73.

A one-dimensional model of a false aneurysm

[1]Fredrik Berntsson, [2]Matts Karlsson, [3]Vladimir Kozlov, [4]Sergey A. Nazarov

[1,2,3] Linköping University, SE-58183 Linköping, Sweden.
[4] St Petersburg State University, St Petersburg State Polytechnical University, and Institute of Problems of Mechanical Engineering RAS, Russia.

Abstract: A false aneurysm is a hematoma, i.e. collection of blood outside of a blood vessel, that forms due to a hole in the wall of an artery . This represents a serious medical condition that needs to be monitored and, under certain conditions, treated urgently. In this work a one-dimensional model of a false aneurysm is proposed. The new model is based on a one-dimensional model of an artery previously presented by the authors and it takes into account the interaction between the hematoma and the surrounding muscle material. The model equations are derived using rigorous asymptotic analysis for the case of a simplified geometry.
Even though the model is simple it still supports a realistic behavior for the system consisting of the vessel and the hematoma. Using numerical simulations we illustrate the behavior of the model. We also investigate the effect of changing the size of the hematoma. The simulations show that our model can reproduce realistic solutions. For instance we show the typical strong pulsation of an aneurysm by blood entering the hematoma during the work phase of the cardiac cycle, and the blood returning to the vessel during the resting phase. Also we show that the aneurysm grows if the pulse rate is increased due to, e.g., a higher work load.

1 Introduction

In this paper we deal with modeling a false aneurysm located on the large femoral artery [24]. The false aneurysm differs from a true aneurysm by the absence of a rigid wall surrounding the hematoma. The false aneurysm appears as a result of blood flow through a hole in vessel's wall. Such a hole can appear due to, e.g., a trauma that punctures the artery, such as knife and bullet wound, or as a result of percutaneous surgical procedures such as coronary angiography or arterial grafting [8], or due to the use of an artery for injecting medicine. A characteristic feature of a false aneurysm is a strong pulsation which is due to abundant blood flow into the hematoma, during the early stages of the cardiac cycle, and its subsequent slow return to the artery due to the compressive stress of the surrounding muscle tissue [1].

The aim of this work is the presentation of the simplest model, that still properly describes the functioning of the vessel/hematoma system. The geometry is maximally simplified: the axis symmetry condition is introduced, the effects of a boundary layer type near the hole are neglected, the surrounding muscle tissue occupies the remaining part of cross-sections $y = (y_1, y_2)$, the vessel wall and the bed vessel are modelled by an elastic two-dimensional surface and the vessels is assumed to be a circular cylinder.

Simplicity of the model is predetermined by requirements of its application. Let us make some comments concerning this issue. First of all, it is impossible to take into account all physical and geometric forms of the objects constituting the biological system under consideration. The blood is a

multi-component liquid with pronounced viscoelastic properties. The vessel wall is a three layer shell strengthen by families of collagen fibers. The elastic material of the muscle is non homogeneous and anisotropic exposing to aging (admitting stress relaxation). The hematoma contains volumes of stagnant and partially clotted blood together with neoplasms and suppuration. Besides the characteristics of the objects essentially depends on external factors, e.g. time of day, temperature, exercise stress, medical drugs, etc. Thus a very detailed analysis is not required. Second, if the results are to be useful to physicians they must be expressed in very simple terms. Also, as open ejection of blood from the femoral artery leads to death within 20-30 minutes, there is a strict time limit involved. Thus we have to rely on average statistical data found in medical textbooks, rather than individual data in our model. Finally, a hematoma on the femoral artery will have an influence of the larger vascular tree. For instance, the first action of the doctor after finding a false aneurysm is to investigate the availability of pulse around the ankle.

The paper is organized as follows: In Section 2 we present the details of our model for the false aneurysm. In Section 3 we give a brief description of our numerical model and also present several experiments intended to illustrate the properties of the aneurysm model. Finally, in Section 4 we discuss the both results and the future direction of our research.

2 The False Aneurysm Model

Consider a segment of the artery in the shape of a circular cylinder

$$\Theta_a = \{x = (y, z) \in \mathbb{R}^2 \times \mathbb{R} \,:\, r = |y| < a, z = x_3 \in (-\ell_-, \ell_+)\}, \tag{1}$$

where $a > 0$ is the radius, $\ell = \ell_+ + \ell_-$ is the length and $\ell_\pm > 0$. The ratio

$$\delta_w = a/\ell \tag{2}$$

is considered as a small parameter. The vessel's wall is modelled as a thin solid cylindrical shell of layer structure; see [7, Chapter11] and [5, Chapter 8]. Due to the averaging and dimensional reduction procedures developed in [13, 12], the vessel wall can be replaced by the elastic two-dimensional surface

$$\Gamma_a = \{(y, z) \,:\, r = a, z \in (-\ell_-, \ell_+)\}. \tag{3}$$

A fusiform aneurysm is an axis-symmetric, oblong domain

$$\Xi_H = \{(y, z) \,:\, a < r < a + H(z), z \in (-L_-, L_+)\}, \tag{4}$$

and its length $L = L_+ + L_- < \ell$, $L_\pm > 0$, and the profile H is a smooth function defined on the closed interval $[-L_-, L_+]$,

$$H(z) > 0 \ \text{ for } z \in (-L_-, L_+), \quad H(\pm L_\pm) = 0, \ \ \partial_z H(\pm L_\pm) \neq 0. \tag{5}$$

The dimensionless parameters

$$\delta_h = \frac{\max H(z)}{\min L_\pm} \ \text{ and } \ h_h = \frac{a}{a + \max H(z)} \tag{6}$$

are also assumed to be small. Moreover, taking into account the anatomical structure we have

$$L_-/\ell_- << 1 \ \text{ and } \ L_+/\ell_+ << 1. \tag{7}$$

Finally, the small hole of the diameter $\mathcal{O}(a)$ is located at $z = 0$.

2.1 Equations of hydrodynamics and elasticity

At this stage, we ignore the hole and consider separately the blood flow in the vessel and in the hematoma. The natural assumption about smallness of the Reynolds and Stokes numbers in the artery:

$$\mathtt{Re}_b = \frac{1}{\nu}\frac{1}{T}al \ \text{ and } \ \mathtt{St}_b = \frac{1}{\nu_b}\frac{1}{T}a^2 = \delta_w \mathtt{Re}_b, \tag{8}$$

allows us to discard the inertial and convective terms in the unsteady Navier-Stokes system and thus we obtain the Stokes system

$$-\nu\Delta v + \nabla p = 0 \ \text{ and } \ -\nabla\cdot v = 0 \ \text{ in } \Theta_a \tag{9}$$

that is intended to describe the blood flow in the artery, cf. [23] and [2, 10, 9]. Here, ∇ is gradient, $\nabla\cdot$ is divergence, $\Delta = \nabla\cdot\nabla$ is the Laplacian, $\nu > 0$ is the coefficient of viscosity, $\mathbf{v}$ is the velocity vector and p is the pressure. Moreover, T denotes the period of heartbeat, i.e. $1/T$ is the pulse rate.

The blood volumes inside the vessel and the hematoma, respectively, are

$$V_v = \pi\ell a^2 \text{ and } V_h = \pi\int_{-L_-}^{L_+}(H(z)+a)^2dx. \tag{10}$$

Since V_h must be, at most, comparable with V_v, otherwise immediate surgery is needed, and $H(z)+a > a$, $L < \ell$, the smallness assumption on the numbers (8) implies that the Reynolds number in the hematoma is also small,

$$\mathtt{Re}_h = \frac{1}{\nu}\frac{1}{T}L\max H(z) \approx \mathtt{Re}_b. \tag{11}$$

Therefore, in view of the smallness of δ_h from (6), the Reynolds number $\mathtt{Re}_h$ and the Stokes number $\mathtt{St}_h = \delta_h\mathtt{Re}_h$ are also small and hence the velocity vector V and the pressure P in the hematoma satisfy the Stokes system

$$-\nu\Delta V + \nabla P = 0 \ \text{ and } \ -\nabla\cdot V = 0 \ \text{ in } \Sigma_H. \tag{12}$$

According to results from [13, 12] the averaged equations for the composite vessel wall, which are written on the surface (3) under the axial symmetry assumptions, have the form

$$K_{\varphi\varphi}a^{-1}u_r + K_{\varphi z}\partial_z u_z + ha\gamma_w\partial_t^2 u_r = \gamma_b(f_r - F_r), \tag{13}$$

$$-hK_{z\varphi}\partial_z u_r - haK_{zz}\partial_z^2 u_z + ha\gamma_w\partial_t^2 u_z = \gamma_b(f_z - F_z) \ \text{ on } \Gamma_a, \tag{14}$$

where u_r and u_z are radial and transversal displacements respectively, f_r, F_r and f_z, F_z are similar components of hydrodynamical forces, i.e.

$$\begin{aligned} f_r &= p + \nu\partial_r v_r, \ \ F_r = P + \nu\partial_r V_r, \\ f_z &= \frac{\nu}{2}(\partial_r v_z + \partial_z v_r), \ \ F_z = \frac{\nu}{2}(\partial_r V_z + \partial_z V_r), \end{aligned} \tag{15}$$

where t is time, h is the relative thickness of the wall, γ_w and γ_b are the densities of the wall (effective) and the blood, respectively, and finally

$$K = \begin{pmatrix} K_{\varphi\varphi} & K_{\varphi z} \\ K_{z\varphi} & K_{zz} \end{pmatrix} \tag{16}$$

is a symmetric and positive definite constant matrix representing the effective elastic moduli for the vessel wall.

Relation (13) means that the hydrodynamical forces acting from different sides of the wall on the vessel wall are balanced by internal stresses together with inertial forces. We note that a one-dimensional model contains only one coefficient

$$K_w = K_{\varphi\varphi} \tag{17}$$

from the stiffness matrix (16). In addition to the system (13) we supply the surface Γ_a with the dynamic no-slip conditions

$$\mathbf{v} = \partial_t \mathbf{u}, \;\; V = \partial_t \mathbf{u}. \tag{18}$$

Consider the following three Womersley numbers

$$\mathtt{W}_b = (\mathtt{St}_b)^{1/2}, \;\; \mathtt{W}_w = \frac{a}{T}\sqrt{\frac{h\gamma_w}{K_w}}, \;\; \mathtt{W}_m = \frac{\max H(z)}{T}\sqrt{\frac{\gamma_m}{K_m}}. \tag{19}$$

The first one is related to fluid and it is small due to our assumptions on numbers (8). Discussion on the second number is postponed to Section 2.2. The third one, containing the density γ_m and the stiffness modulus K_m of the surrounding muscle material, is small due to a similar argument as the one in the papers [9, 10].

The transversal size of the surrounding muscle material must significantly exceed the length and diameter of the hematoma. If this is not the case then the situation is super critical and urgent surgical intervention is required. We assume that the system $\Theta_a \cup \Sigma_H$ is located inside an infinite muscle layer $\{x \,:\, y \in \mathbb{R}^2, z \in (-L_-, L_+)\}$, which is a transversely isotropic elastic material. In other words, the reaction of the surrounding material on the artery itself can be neglected. Damping out external influences is the purpose of the loosened vascular layer, that is the vessel bed, see the discussion in [9, 10]. However as follows from the definition of the false aneurysm hematoma equilibrium is supported exclusively by muscle resistance.

The external boundary of the hematoma

$$\Upsilon_H = \{(y, z) \,:\, r = a + H(z), z \in (-L_-, L_+)\} \tag{20}$$

in the false aneurysm is separated from the surrounding muscle material by a very thin film. The reaction on the muscle material from the hydrodynamical force

$$F = \gamma_b P N + \gamma_b \nu E \cdot N \;\text{ on } \Upsilon_H \tag{21}$$

represents the traction $T = \Sigma \cdot N$, compare with (15), where $E = (E_{jk})$ is the tensor of deformation velocities,

$$E_{jk} = \frac{1}{2}\Big(\frac{\partial V_j}{\partial x_k} + \frac{\partial V_k}{\partial x_j}\Big), \quad j, k = 1, 2, 3, \tag{22}$$

$\Sigma = (\Sigma_{jk})$ is the tensor of stresses in the muscle material and N is the unit vector of outward normal to the surface (20),

$$N = (1 + |\partial_z H(z)|^2)^{-1/2}\big((a + H(z))^{-1} y_1, (a + H(z))^{-1} y_2, -\partial_z H(z)\big). \tag{23}$$

We ignore other effects that impact the boundary of the hematoma and thus we arrive at the following boundary condition

$$\Sigma \cdot N + \gamma_b P N + \gamma_b \nu E \cdot N = 0. \tag{24}$$

2.2 Dimension reduction procedure

We start with the one-dimensional Reynolds equation for blood flow in a thin vessel; see details in [9, 10]. We consider separately the two parts of the vessel: $\Theta_a^{\pm} = \{(y, z) \,:\, \pm z \in (0, \ell_{\pm})\}$; that is before and after the hole. A rigorous asymptotic analysis, see [10, 23, 20], shows that the leading term of the pressure $p(y, z)$ does not depend on the transversal variables $y = (y_1, y_2)$ and the longitudinal component of the velocity vector prevails over the transversal components $v' = (v_1, v_2)$. Concerning the displacement components of the wall of the artery, the radial component u_r dominates over the longitudinal one, u_z.

Taking into account the above observations and slow variability of fields in the direction z, we arrive at the following problem on the cross-section $\mathbb{B}_a = \{y \in \mathbb{R}^2 : r < a\}$ of the vessel:

$$\nu\Delta_y \overline{v}_z(y,z,t) = \partial_z \overline{p}(z,t), \quad y \in \mathbb{B}_a, \quad \overline{v}_z(y,z,t) = 0, \quad y \in \partial\mathbb{B}_a. \tag{25}$$

Its solution is given by

$$\overline{v}_z(y,z,t) = \frac{1}{4\nu}(r^2 - a^2)\partial_z \overline{p}(z,t). \tag{26}$$

Also, we calculate the flux through the cross section:

$$\overline{\varphi}(z,t) = \int_{\mathbb{B}_a} \overline{v}_3(y,z,t)dy = -\frac{\pi a^4}{8\nu}\partial_z \overline{p}(z,t). \tag{27}$$

The over lined quantities corresponds to the leading terms of corresponding quantities.

Among remaining relations in (9) and (18) we need the following consequences of the continuity equation and the dynamic no-slip condition

$$-\nabla_y \cdot \overline{v}'(y,z,t) = \partial_z \overline{v}_3(y,z,t), \quad y \in \mathbb{B}_a, \tag{28}$$

and

$$\overline{v}'_r(y,z,t) = \partial_t u_r(z,t), \quad y \in \partial\mathbb{B}_a. \tag{29}$$

Applying integration by parts to $\int_{\mathbb{B}_a} \nabla_y \cdot \overline{v}' dy$, we obtain

$$2a\partial_t \overline{u}_r(z,t) - \frac{a^4}{8\nu}\partial_z^2 \overline{p}(z,t) = 0, \quad z \in (-\ell_-, 0) \cup (0, \ell_+). \tag{30}$$

According to the dimensional reduction procedure for a thin slightly curved three-dimensional channel with variable cross-section, similar properties have the solution $\{V, P\}$ of the Stokes system (12) for the hematoma. At the same time, smallness of h_h, see (6), with respect to the diameter of the vessel in the hematoma, allows us to replace the ring $\mathbb{B}_{a+H(z)} \setminus \mathbb{B}_a$ by the punctured circle $\mathbb{B}_{H(z)}$ and the corresponding solution to the Dirichlet problem, see (25), in this ring by solution of the problem in the circle similar to (26):

$$\overline{V}_z(y,z,t) = \frac{1}{4\nu}(r^2 - H(z)^2)\partial_z \overline{P}(z,t). \tag{31}$$

It should be emphasized that the asymptotic analysis performed in [14, Ch. 12-13] shows that the accuracy due to replacement of the ring by a circle is of order $O(|\log h_h|^{-1})$ and it increases when $z \to \pm L_\pm$. However, in order to simplify the final model, having in mind many disregarded factors, we neglect also these details. As a result, the flux through the cross-section of the hematoma can be evaluated according to

$$\overline{\Phi}(z,t) = \int_{\mathbb{B}_{H(z)}} \overline{V}_z(y,z,t)dy = -\frac{\pi H(z)^4}{8\nu}\partial_z \overline{P}(z,t). \tag{32}$$

Using the same scheme as in [10, 23, 20], we continue the procedure of dimensional reduction. The continuity equation in the Stokes system (12) gives the relation

$$-\nabla_y \cdot \overline{V}'(y,z,t) = \partial_z \overline{V}_z(y,z,t), \quad y \in \mathbb{B}_{H(z)}. \tag{33}$$

It remains to determine a boundary condition on $\partial\mathbb{B}_{H(z)}$.

The assumption on the Womersley numbers in (19), smooth variability of the hematoma in the z direction and its small relative thickness allow us to reduce the analysis to solving a two-dimensional

elasticity problem on the plane with a circular hole for determination of the muscle reaction on implementation and increase of the hematoma. Such axis-symmetric solution is known, see [22, vol. 2, sec. 11.2]:

$$w_r(r,\varphi) = cr^{-1}, \;\; w_\varphi(r,\varphi) = 0, \\ \sigma_{rr}(r,\varphi) = -2\mu c r^{-2}, \;\; \sigma_{\varphi\varphi}(r,\varphi) = 2\mu c r^{-2}, \;\; \sigma_{r\varphi}(r,\varphi) = \sigma_{\varphi r}(r,\varphi) = 0. \tag{34}$$

The polar coordinates r, φ are used here together with the components of two-dimensional displacement vector w and corresponding stress tensor. Here μ is the shear modulus for transverse isotropic muscle material.

Since the surrounded muscles adapt to the inclusions after certain time, i.e. relaxation of stresses occurs and it is caused by dislocation, it is reasonable to take the middle position of the exterior boundary of the hematoma as the reference surface. The traction applied from the muscle material, we represent as the sum $T^H + T^P$, where T^H is the traction due to the radial dislocation $H(z)$ and T^P is the traction doe to the increase $\overline{U}_r(z,t)$ of the radius of hematoma because of the internal blood pressure. Applying formulae (34) with $c^H = H(z)(a + H(z))$ and $c^P = \overline{U}_r(z,t)(a + H(z))$ respectively we obtain that

$$T_r^H(z,t) = -2\mu \frac{H(z)}{a + H(z)} \approx -2\mu, \tag{35}$$

$$T_r^P(z,t) = -2\mu \frac{\overline{U}_r(z,t)}{a + H(z)} \approx -2\mu H(z)^{-1} \overline{U}_r(z,t) \tag{36}$$

and the components T_φ^H, T_z^H and T_φ^P, T_z^P are neglectable. In (35), the smallness of the second parameter in (6) is used.

The above-listed properties of the blood flow $\{V, P\}$ show the the hydro-dynamic forces on the surface Υ_H are subject to the relations

$$F_r \approx \overline{P}, \;\; F_\varphi \approx 0, \;\; \text{and} \;\; F_z \approx 0. \tag{37}$$

Moreover, the normal vector (23) on Υ_H is approximately equal to $(y_1/r, y_2/r, 0)$. As a result, the boundary condition (24) transforms into

$$\gamma_b \overline{P}(z,t) = 2\mu + 2\mu H(z)^{-1} \overline{U}_r(z,t) \tag{38}$$

and the dynamic no-slip condition on Υ_H becomes

$$\overline{V}'(z,t) = \partial_t \overline{U}_r(z,t) = \frac{\gamma_b}{2\mu} H(z) \partial_t \overline{P}(z,t).$$

Let us sum up intermediate results. As in the case of (28)–(30), calculation of the flux in the cross-section $\mathbb{B}_{H(z)}$ according to (33) and (38) leads to one-dimensional equation for the blood flow in the hematoma:

$$\frac{\gamma_b}{\mu} H(z)^2 \partial_t \overline{P}(z,t)) - \frac{1}{8\nu} \partial_z (H(z)^4 \partial_z \overline{P}(z,t)) = 0, \;\; z \in (-L_-, 0) \cup (0, L_+). \tag{39}$$

Similar to [10], it remains to note that $f_r \approx \gamma_b \overline{p}$ and derive from the first line in (13) one-dimensional equation for oscillations of the wall of artery:

$$K_w a^{-1} \overline{u}_r(z,t) + ha\gamma_w \partial_t^2 \overline{u}_r(z,t) = \gamma_b (\overline{p}(z,t) - \overline{P}(z,t)), \;\; z \in (-L_-, 0) \cup (0, L_+). \tag{40}$$

The second line in (13) contains terms that are small with respect to (40) and therefore we do not take them into account in our one-dimensional model.

2.3 Statement of boundary and other conditions

The hole in the wall of artery equalizes pressure in the vessel and hematoma at the location $z = 0$, i.e. the one-dimensional equation must be supplied with the transmission Kirchhoff conditions

$$\overline{p}(+0,t) = \overline{p}(-0,t) = \overline{P}(+0,t) = \overline{P}(-0,t). \tag{41}$$

In other words, the functions $\overline{p}$ and $\overline{P}$ are continuous and take the same value at $z = 0$. The other Kirchhoff condition means that the sum of fluxes at $z = 0$ vanishes, i.e. according to (27) and (32), we have

$$\frac{a^4}{8\nu}[\partial_z\overline{p}](t) + \frac{H(0)^4}{8\nu}[\partial_z\overline{P}](t) = 0, \tag{42}$$

where $[q](t) = q(+0,t) - q(-0,t)$ is the jump of the function q at the point $z = 0$.

Now let us turn to the formulation of boundary conditions. Due to the geometrical assumptions (5) coefficients of the differential equation (39) degenerate at the points $z = \pm L_{\pm}$ and therefore this equation does not need boundary condition. It is sufficient to require continuity of $\overline{P}$ on the interval $[-L_-, L_+]$; see [15, sec. 30] and [19] concerning asymptotical analysis of thin domains with sharp edges.

As usual in modeling of blood flow in vessel one ought to prescribe the flux at the input $x = -\ell_-$, i.e. according to formula (27) we obtain the Neumann condition

$$-\frac{a^4}{8\nu}\partial_z\overline{p}(-\ell_-,t) = \frac{1}{\pi}\overline{\varphi}_0(t), \tag{43}$$

where $\varphi_0(t)$ is the real blood flux sent by the heart at the time moment t.

At the remote output $x = \ell_+$, located at the ankle level, it is reasonable to prescribe peripheral pressure p_∞, which can be considered to be constant. Nevertheless, pay attention to two facts. First, the constant pressure

$$P_0 = 2\mu/\gamma_b, \tag{44}$$

caused by the static reaction of the muscle on filling in of the hematoma, does not occur in equations (30), (39), (40) and conditions (41)-(43). Second, the pressure (44) is small with respect to the second term $2\mu\gamma_b^{-1}H(0)^{-1}\overline{U}_r(z,t)$ in (38) in the active phase of blood flow sent by the heart through the level $z = 0$, but it acts during sufficiently long period of the passive phase. One of simple methods of accounting such constant pressure is to change variables

$$\overline{P}(z,t) \mapsto \overline{P}(z,t) - P_0 \ \text{ and } \ \overline{p}(z,t) \mapsto \overline{p}(z,t) - P_0, \tag{45}$$

which do not influence the above equations and other conditions. Thus preserving the same notation for the just introduced differences (45), we put the following Dirichlet condition

$$\overline{p}(\ell_+,t) = p_\infty - P_0. \tag{46}$$

The hyperbolic equation (40) requires two periodicity conditions

$$\overline{u}_r(z,0) = \overline{u}_r(z,TN), \ \ \partial_t\overline{u}_r(z,0) = \partial_t\overline{u}_r(z,TN). \tag{47}$$

Here, $1/T$ is the pulse rate and N is a natural number. The need to monitor several periods (N) is due to the fact that elastic oscillations of vessel wall are not connected with the rhythm of the heartbeat and, moreover, is regulated by external factors. However, for a young and healthy artery the Womersley number $\mathtt{W}_w$ defined in (19) is small, i.e. inertial term can be withdrawn from equation (40) and the periodicity condition (47) becomes unnecessary.

Equation (40) without inertial term gives the relation

$$\overline{u}_r(z,t) = \frac{\gamma_b}{K_w}a(\overline{p}(z,t) - \overline{P}(z,t)), \tag{48}$$

which converts equation (30) into

$$\frac{2\gamma_b}{K_w}a^2(\partial_t\overline{p}(z,t)-\partial_t\overline{P}(z,t))-\frac{a^4}{8\nu}\partial_z^2\overline{p}(z,t)=0,\ z\in(-\ell_-,0)\cup(0,\ell_+). \tag{49}$$

Clearly, the equation (49) does not require any periodicity condition of the type (47).

2.4 Growth of the hematoma

An increment of the hematoma volume $\triangle\mathcal{V}(t)$ at the moment t is calculated according to the formula

$$\pi\int_{-L_-}^{L_+}\Big((a+H(z)+\overline{U}_r(z,t))^2-(a+H(z)^2\Big)dz\approx 2\pi\int_{-L_-}^{L_+}H(z)\overline{U}_r(z,t)dz.$$

With that according to relation (38), we have

$$\triangle\mathcal{V}(t)=\pi\frac{\gamma_b}{\mu}\int_{-L_-}^{L_+}H(z)^2\overline{P}(z,t)dz. \tag{50}$$

Equation (39) together with the Kirchhoff conditions (41), (42) shows that

$$\begin{aligned}\triangle\mathcal{V}(t)-\triangle\mathcal{V}(0)&=\pi\frac{\gamma_b}{\mu}\int_0^t\int_{-L_-}^{L_+}H(z)^2\partial_t\overline{P}(z,t)dzdt\\&=\frac{\pi}{8\nu}\int_0^t\int_{-L_-}^{L_+}\partial_z(H(z)^4\partial_z\overline{P}(z,t))dzdt=-\frac{\pi}{8\nu}H(0)^4\int_0^t[\partial_z\overline{P}(z,t)]dt.\end{aligned} \tag{51}$$

The total blood flow into the hematoma for the time interval $(0,t)$ appeared in the right hand side of (51). Thus we can monitor the growth of the hematoma during a given time period.

Note though that as our model is linear any growth of the hematoma can be reversed. Also for any periodic solution the net growth over the whole period is always zero. Thus our model does not contain any internal mechanism for permanently increasing the size of the Hematoma, i.e. changing the profile $H(z)$.

3 Numerical implementation and simulations

In this section we discuss our numerical implementation for solving the equations of our model. Numerical simulations of blood flow in veins or arteries have been carried out by several authors, see e.g. [18, 16, 3, 4, 17]. In our previous work [2] we showed that our model for blood flow in arteries could be solved with a simple and very efficient numerical method. In the case of an artery with a hematoma attached the situation is similar.

For our numerical tests we discretize the equations (30), (39), and (40), using the finite difference method. Introduce an equidistant grid $\{z_i\}_{i=1}^N$ on the interval $-\ell_-\le z\le\ell_+$, and a grid $\{t_j\}_{j=0}^M$ on the interval $0\le t\le T$. The unknowns are the pressure $\overline{p}(z_i,t_j)$ in the vessel, the pressure $\overline{P}(z_i,t_j)$ in the hematoma, and the displacement $u_r(z_i,t_j)$ of the vessel's wall. We also introduce $v(z_i,t_j)=\partial_t\overline{u}_r(z_i,t_j)$ as additional unknowns.

Introduce three indicies as follows: $z_{i_1}=-L_-$, $z_{i_2}=0$ and $z_{i_3}=L_+$. The hole is located at the grid point z_{i_1} where u_r and v are undefined. Further, the pressure $\overline{P}(z_i,t)$ is only defined for indicies $i_1\le i\le i_3$. Thus the total number of unknowns at each time step is $3N+i_3-i_1-2$.

In order to satisfy both the partial differential equations, and the extra conditions (41) and (42) at the hole, we formulate an implicit time stepping method. For instance from (40) we obtain,

$$K_wa^{-1}\overline{u}_r(z_i,t_{j+1})+\frac{ha\gamma_w}{\Delta t}(v(z_i,t_{j+1})-v(z_i,t_j))=\gamma_b(\overline{p}(z_i,t_{j+1})-\overline{P}(z_i,t_{j+1})), \tag{52}$$

Physical Quantity	Symbol	Unit	Value
Density of walls	γ_w	kg/m^3	1050
Viscosity of blood	ν	$kg/m\,s$	$5.1 \cdot 10^{-3}$
Shear modulus for muscle tissue	μ	Pa	$2.94 \cdot 10^4$
Radius of vessel	a	m	$4.1 \cdot 10^{-3}$
Relative thickness of wall	h		0.16
Modulus of Elasticity of walls	$K_{\varphi\varphi}$	Pa	$4.15 \cdot 10^5$

Table 1: The physical parameters that were used for our tests. The values roughly correspond to the *femoral artery* of a healthy individual.

Aneurysm	$H_1(z)$	$H_2(z)$	$H_3(z)$
$L_\pm\,[cm]$	2.0	2.5	3.0
$\max H(z)\,[mm]$	3.7	4.0	4.2

Table 2: The physical dimensions of the three aneurysm profiles used for our tests.

for $i_1 \leq i \leq i_3, i \neq i_2$, where the implicit Euler method was used to discretize the time derivative. Similarly the Kirchhoff condition (42) is discretized using a second order accurate difference approximation at time $t = t_{j+1}$. The equation (31) is discretized using a second order accurate discretization in space and the implicit Euler method, i.e. we get

$$2a\left(\overline{u}_r(z_i, t_{j+1}) - \overline{u}_r(z_i, t_j)\right) = \frac{a^4}{8\nu}\left(\overline{p}(z_{i-1}, t_{j+1}) - 2\overline{p}(z_i, t_{j+1}) + \overline{p}(z_{i+1}, t_{j+1})\right), \tag{53}$$

for $1 < i < N, i \neq i_2$. The other equations and boundary conditions are treated similarly and we obtain a large sparse linear system to solve for the unknowns at time $t = t_{j+1}$. The finite difference scheme is second order accurate in space and first order accurate in time. Since the model is one-dimensional the number of unknowns are relatively small and solving the equations by direct methods is feasible.

3.1 Numerical simulations

In order to demonstrate that our model works well in practice, and can produce realistic solutions, we give the results from several numerical simulations. As a basis for our calculations we use typical physical parameters that roughly correspond to the femoral artery for a healthy individual; see [21].

In our model we need to specify the shape of the aneurysm. We use three different shapes $H_1(z)$, $H_2(z)$ and $H_3(z)$. The shapes are seen in Figure 1; see also Table 2 for the exact dimensions of the shape functions. The flow velocity profiles used for the boundary condition (43) were taken to be realistic. In the case of a normally working heart an experimental velocity profile $\Phi_1(t)$ was found in [6]. In addition we created an artificial flow profile $\Phi_2(t)$ intended to correspond to a slightly elevated pulse rate. Both flow profiles can be seen in Figure 1. In order to avoid the influence from transient effects and reach a periodic state we set the boundary flow $\Phi(t)$ by first taking 10 copies of $\Phi_1(t)$, followed by 10 copies of $\Phi_2(t)$ and finally another 10 copies of $\Phi_1(t)$. At the boundary $z = L_+$ we used a constant pressure $\overline{p} = p_\infty$, where $p_\infty = 80\,mmHg$, or $10.7\,kPa$. For the space discretization we used $N = 500$ grid points and for the time discretization consisting of $M = 14820$ grid points was used. The time grid covers all 30 heart beats which is a total duration of $26.54\,s$. Due to the fine discretization the equations are solved very accurately.

The goal for our numerical simulations is to study how the hematoma influences the blood flow in the system. In particular we investigate the effect of different aneurysm shapes. The numerical scheme

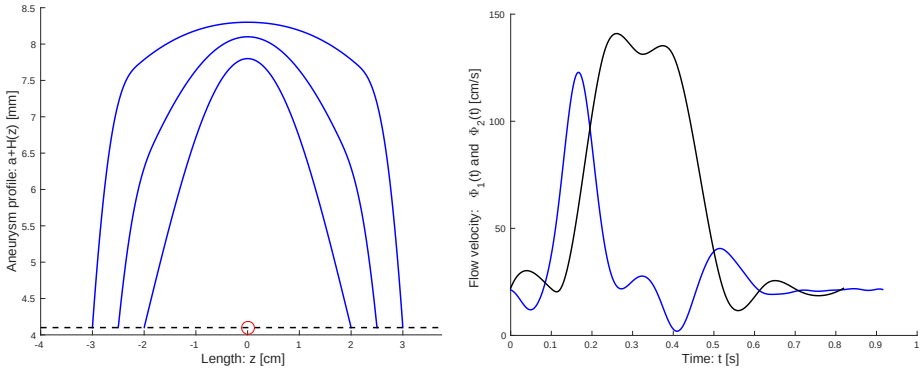

Figure 1: We present the three Aneurysm profiles $H_1(z)$, $H_2(z)$ and $H_3(z)$ (left graph). The function $H_1(z)$ represents the smallest aneurysm and $H_3(z)$ is the largest. Note the different scales on the vertical and horizontal axes in the graph. We also display the flow velocity profiles at the inlet $z = -L_-$ (right graph). The function Φ_1 (blue curve) corresponds to a normal case with a pulse rate of $T_1 = 0.917\,s$. The profile Φ_2 (black curve) correspond to an elevated work load and $T_2 = 0.820\,s$.

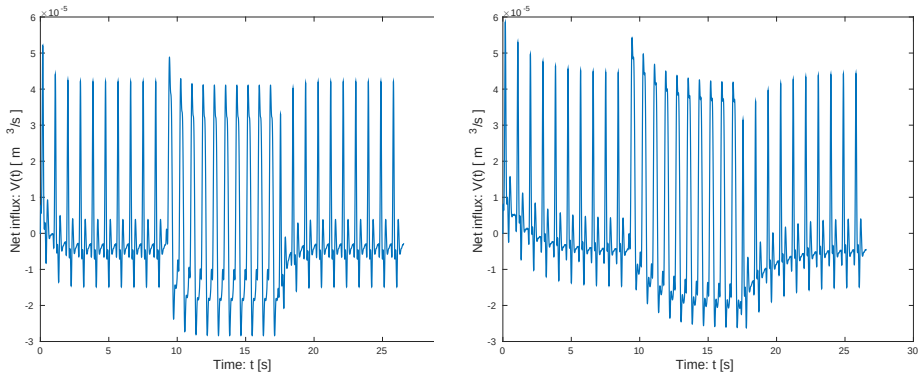

Figure 2: The net influx of blood into the hematoma during the simulations for the cases when the aneurysm profile is given by $H_1(z)$ (left) and $H_3(z)$ (right). For the larger hematoma it takes longer for the calculations to reach steady state. In both cases 10 heart beats is enough for the system to reach a periodic solution.

requires us to specify initial conditions. In our experiments we use a zero solution as the initial state of the system which means no blood flow. During the first few heart beats the hematoma is filled with blood. This is seen in Figure 2 where the net-influx into the hematoma is illustrated. The larger hematoma profile $H_3(z)$ requires about six heart beats for the blood flow to reach a periodic state. Note that after 10 heart beats the influx condition changes to the elevated work load. This means the hematoma grows; which is seen as a positive net influx of blood. After 20 heart beats the work load returns to normal and the hematoma shrinks back to its original size. In Figure 3 we see the net influx during one of the normal heart beats and during one of the elevated work load heart beats.

In order to illustrate the effect of the hematoma we show flow velocity profiles taken at $z = \pm 11\,mm$, i.e. before and after the hematoma. The results are displayed in Figure 4. We see that the hematoma has a very small influence on the flow velocity at $z = -11\,mm$. The velocity profiles are very close to the prescribed boundary data. After the hematoma, i.e. at $z = 11\,mm$ there is a clear difference. During the

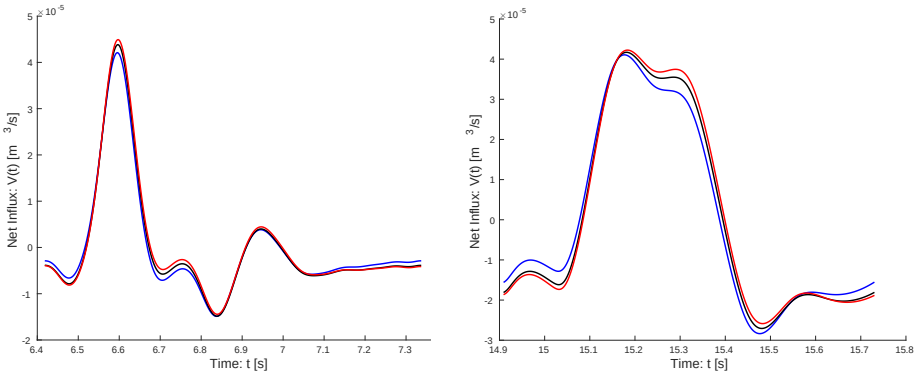

Figure 3: The net influx of blood into the hematoma during one of the normal heart beats (left graph) and during one of the work heart beats (right graph). In both cases we display the cases when the hematoma is given by $H_1(z)$ (blue curve), $H_2(z)$ (black curve), and $H_3(z)$ (red curve). During the work phase more blood enters and leaves the Hematoma during the heart beat. Also the size of the hematoma has a slightly bigger effect.

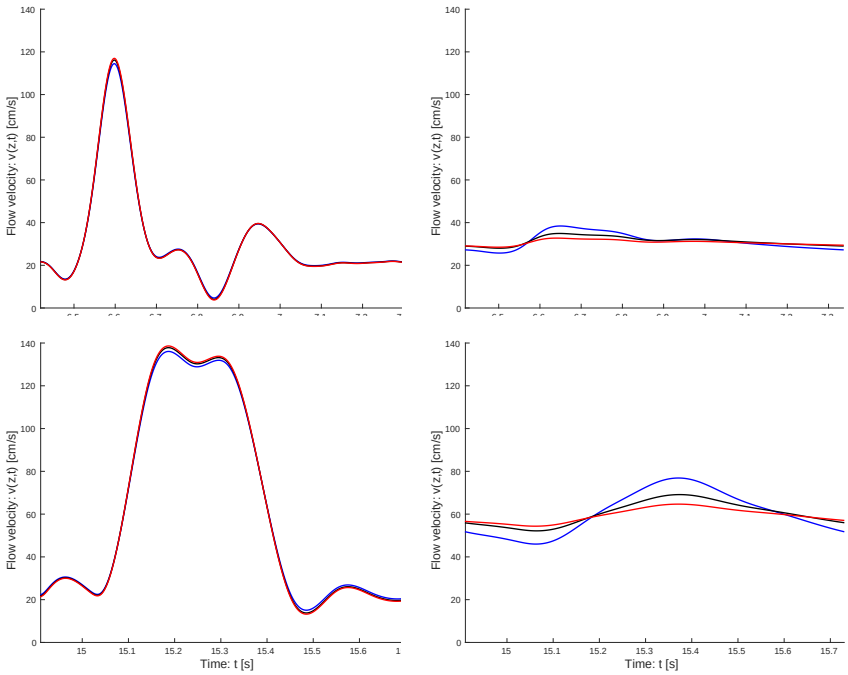

Figure 4: Flow velocity profiles $v(z,t)$ at $z = -11\,mm$ (left graphs) and at $z = 11\,mm$ (right graphs) in the case of the normal heart beat (top graphs) and the case of an elevated work load (bottom graphs). In both cases we display the cases when the hematoma is given by $H_1(z)$ (blue curve), $H_2(z)$ (black curve), and $H_3(z)$ (red curve). We note that the hematoma has very little effect on the flow before $z = 0$. After the hematoma, i.e. for $z > 0$, the flow velocity is evened out. This is due to the hematoma acting as a reservoir. The effect is strongest for the larger hematoma.

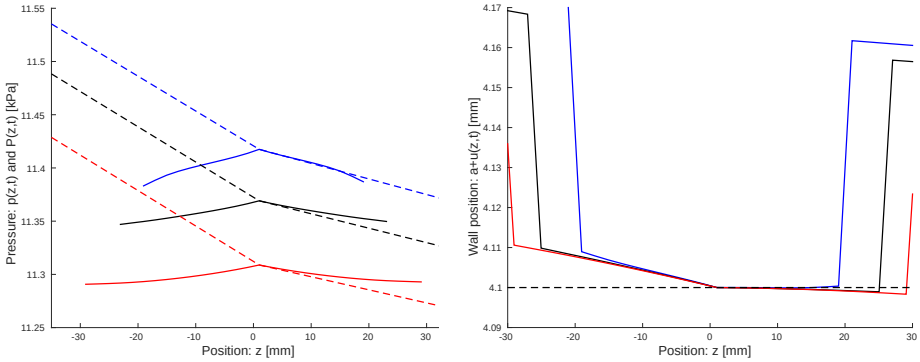

Figure 5: The pressure profiles $p(z,t)$ and $P(z,t)$ at time $t = 11.1\,s$ (left graph). This is during a elevated work heart beat when the influx velocity profile $\Phi_2(t)$ reaches its maximum. Also the corresponding wall positions $a + u(z,t)$ near the hematoma (right graphs). In all cases the hematoma is given by $H_1(z)$ (blue curve), $H_2(z)$ (black curve), and $H_3(z)$ (red curve). Note that the pressure inside the blood vessel, i.e. $p(z,t)$, changes faster than the pressure $P(z,t)$ inside the hematoma. This means that for $z > 0$ the pressure inside the Hematoma is larger than the pressure in the vessel. Hence $u(z,t) < 0$ and the vessel is reduced in radius.

work phase the hematoma is filled with blood; and that blood is returned to the vessel during the resting phase. This means that the hematoma acts as a reservoir that evens out the flow of blood during the heart cycle. This is consistent with the observation that, in practice, it is difficult to feel a clear pulse after a hematoma on patients. This effect is strongest for the larger hematoma.

Finally, we illustrate the pressure profiles $\overline{p}$ and $\overline{P}$ at time $t = 11.1\,s$. The time instance $t = 11.1\,s$ corresponds to when the flow profile $\Phi_2(t)$ reaches its peak. We see that the pressure changes more slowly inside the hematoma than in the vessel. As a consequence the wall displacement $\overline{u}_r$ is positive for $z < 0$ and negative for $z > 0$. This means that after the hole $P > p$ and the vessels effective radius $a + \overline{u}_r < a$. Thus the hematoma effectively hinders the blood flow. This effect is also stronger for the larger hematoma size.

4 Concluding Remarks

In this paper we have presented a one dimensional model of a false aneurysm. The model is derived from the original three dimensional flow equations by dimension reduction and asymptotical analysis, cf. [10, 11], and the geometry has been simplified as much as possible. In order to illustrate the behavior of the model we also present numerical simulations using a simple finite difference code for solving the partial differential equations. The code is implicit as this makes it easier to enforce Kirchhoff type transmission conditions at the hole that connects the vessel and the aneurysm. Though, if a periodic solution is sought, a direct solver based on solving the equations in the frequency domain also works, see our previous paper [2].

From the numerical simulations we make several observations about our model. First the heart beat cycle is divided into a work phase, where the heart keeps up pressure, and a resting phase. During the work phase the aneurysm increases in size as a fraction of the blood flow in the vessel is diverted through the hole. During the resting phase the blood is returned into the vessel. Thus the aneurysm acts as a reservoir that evens out the blood flow during the whole cardiac cycle. This behavior is consistent with the observation that it is difficult to feel a clear pulse in patients suffering from having a false aneurysm on an artery.

Pressure profiles from the vessel and the aneurysm indicates that the pressure gradient is smaller inside the aneurysm. This means a mostly stagnant flow except for a region near the hole. Also the vessel clearance shrinks after the hole due to the pressure in the aneurysm being higher than the pressure inside the artery. This might hinder the blood flow.

The geometry of the model is the simplest possible with a straight vessel having a circular cross section. The radius a represents a typical radius at a normal working pressure, and the model is linearized around this typical situation. In practice the typical radius of the artery would be change due to the influence of the hematoma and a constant value a for the entire length of the vessel is not realistic. This is an aspect of the model we intend to improve in the near future.

Furthermore, as the model is linear, the aneurysm always remains stable in the model. The size of the aneurysm can increase by altering the heart beat, but if the heart beat returns to normal so does the size of the aneurysm. Including a mechanism that permanently changes the shape of the aneurysm, i.e. the function $H(z)$, during the simulations, is also a topic we intend to explore in the future.

References

[1] R. J. Baird and M. L. Doran. The false aneurysm. *Canadian Medical Association Journal*, 91(6):281284, 1964.

[2] Fredrik Berntsson, Matts Karlsson, Vladimir Kozlov, and Sergey A. Nazarov. A one-dimensional model of viscous blood flow in an elastic vessel. *Applied Mathematics and Computation*, 274:125–132, 2016.

[3] V. Casulli, M. Dumbser, and E. F. Toro. Semi-implicit numerical modeling of axially symmetric flows in compliant arterial systems. *Int. J. Numer. Meth. Biomed. Engng.*, 28:257–272, 2012.

[4] F. Fambri, M. Dumbser, and V. Casulli. An efficient semi-implicit method for three-dimensional non-hydrostatic flows in compliant arterial vessels. *Int. J. Numer. Meth. Biomed. Engng.*, 30:1170–1198, 2014.

[5] Y.C. Fung. *Biomechanics: mechanical properties of living tissues*. Springer-Verlag, 1993.

[6] D W Holdsworth, C J D Norley, R Frayne, D A Steinman, and B K Rutt. Characterization of common carotid artery blood-flow waveforms in normal human subjects. *Physiological Measurement*, 20(3):219, 1999.

[7] G.A. Holzapfel. *Collagen. Structure and Mechanic*, chapter Ch. 11. Collagen in Arterial Walls: Biomechanical Aspects, pages 285–324. Springer-Verlag, 2008.

[8] Morton L. Kern, Paul Sorajja, and Michael Lim. *Cardiac Catheterization Handbook*. Elsevier, 6ed edition, 2015.

[9] V. A. Kozlov and S. A. Nazarov. An asymptotic model of the interaction of blood flow with vein walls and the surrounding muscle tissue. *Dokl. Akad. Nauk*, 446(6):631–636, 2012. English transl.: Doklady Physics, 2012, V. 57, N 10. P. 411–416.

[10] V. A. Kozlov and S. A. Nazarov. Asymptotic models of blood flow in arteries and veins. *Zap. Nauchn. Sem. S.-Peterburg. Otdel. Mat. Inst. Steklov. (POMI)*, 409(Matematicheskie Voprosy Teorii Rasprostraneniya Voln. 42):80–106, 242, 2012. English translation: Journal of Math. Sci., 2013, vol. 194, no. 1, pp. 44–57.

[11] V. A. Kozlov and S. A. Nazarov. An elementary on-dimensional model of a false aneurysm in the large femoral artery. *Zap. Nauchn. Sem. S.-Peterburg. Otdel. Mat. Inst. Steklov. (POMI)*, 426:64–86, 2014.

[12] V. A. Kozlov and S. A. Nazarov. Asymptotic models of anisotropic heterogeneous elastic walls of blood vessels. *Probl. mat. analiz.*, 83:101–127, 2015. English translation: Journal of Math. Sci., 2016., Vol. 213, No. 4., pp. 561-581.

[13] Vladimir Kozlov and Sergei Nazarov. Surface enthalpy and elastic properties of blood vessels. *Doklady physics*, 56(11):560–566, 2011.

[14] V. Maz'ya, S. Nazarov, and B. Plamenevskij. *Asymptotic Theory of Elliptic Boundary Value Problems in Singularly Perturbed Domains*, volume 2 of *Operator Theory: Advances and Applications*. Birkhäuser Basel, 2000.

[15] S. G. Mikhlin. *Variational methods in mathematical physics*. Pergamon Press, New York, 1964. Translated by T. Boddington; editorial introduction by L.I.G. Chambers.

[16] L. O. Mller and E. F. Toro. Well-balanced high-order solver for blood flow in networks of vessels with variable properties. *Int. J. Numer. Meth. Biomed. Engng.*, 29:13881411, 2013.

[17] L. O. Mller and E. F. Toro. Enhanced global mathematical model for studying cerebral venous blood flow. *Journal of Biomechanics*, 47:3361–3372, 2014.

[18] Lucas O. Mller, Carlos Pars, and Eleuterio F. Toro. Well-balanced high-order numerical schemes for one-dimensional blood flow in vessels with varying mechanical properties. *Journal of Computational Physics*, 242(0):53–85, 2013.

[19] S. A. Nazarov and J. Taskinen. Asymptotics of the solution to the neumann problem in a thin domain with sharp edge. *Journal of Mathematical Sciences*, 142(6):2630–2644, 2007.

[20] S.A. Nazarov and K.I. Pileckas. Reynolds flow of a fluid in a thin three-dimensional channel. *Litovsk. mat. sbornik.*, 30(4):772–783, 1990. English transl.: Lithuanian Math. J. 1990. Vol. 30, No. 4., pp. 366-375.

[21] Niema M Pahlevan and Morteza Gharib. Aortic wave dynamics and its influence on left ventricular workload. *PLoS One*, 6(8):e23106, 2011.

[22] L.I. Sedov. *Mechanics of Continuous Media: (In 2 Volumes)*. Series in Theoretical and Applied Mechanics. World Scientific, 1997.

[23] Canic Suncica and Mikelic Andro. Effective equations modeling the flow of a viscous incompressible fluid through a long elastic tube arising in the study of blood flow through small arteries. *SIAM J. Appl. Dyn. Syst.*, 2(3):431–463, 2003.

[24] Paul V Tisi and Michael J Callam. Treatment for femoral pseudoaneurysms. *Cochrane Database of Systematic Reviews*, (2), 2009.